Bachelor Thesis

Phonon-Magnon coupling in $YMnO_3$ crystal

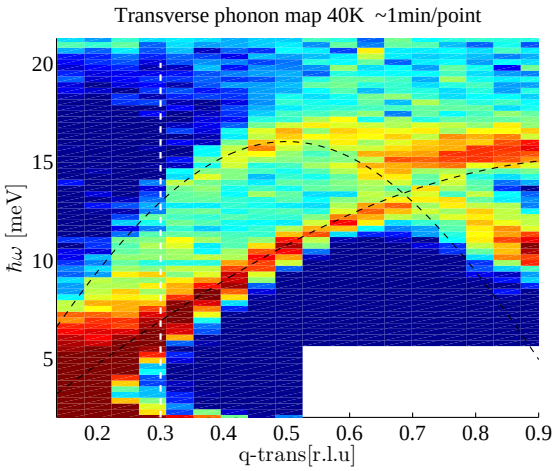

Author: Anders Bakke

Niels Bohr Institute
University of Copenhagen
11. juni 2013

Supervisors: Kim Lefmann and Sonja Lindahl Holm

Preface

This thesis is written as to a bachelor student on his/her final year on the Niels Bohr Institute, University of Copenhagen, Physics. I have assumed that the student has followed the compolsury courses issued from the institute, and has had an Introduction to Solid-State Physics course, similar to that offered by the Niels Bohr Institute.
Most of the theory and experimental method described in this project are covered by the master courses; 'Magnetism and Magnetic Materials', and 'Neutron Scattering'. I do not assume the reader to have knowledge of these subjects, and relevant theory from these courses will be presented throughout the thesis.
Measurements on the EIGER triple-axis spectrometer was taken in cooperation with Jacob Larsen, ph.d student, DTU, Denmark, and my supervisor Sonja Lindahl Holm, ph.d student, KU, Denmark. I attended to these measurements. I was not present during measurements on the RITA2, triple-axis spectrometer. These measurements were done by the attending students on the Neutron Scattering course, summer 2012.

Acknowledgements

First I want to thank to my supervisor, and assoc.prof. Kim Lefmann. Thank you for granting me the opportunity to study in your research group, which has given me strong allies and friends in my later studies. Thank you for the great help and planning throughout the work on my thesis, and for our fruitful discussions.
My deepest thanks and commendations to my second supervisor Sonja Lindahl Holm, for great instructions and guidance throughout the thesis. Thank you for being accesible through the thesis period when I needed help or consultation.
And last I would like to thank the great people in D311, on my campus, for their help with both my thesis and magnetism studies.

Indhold

Abstract and Resume

Abstract

In this thesis we investigate possible phonon-magnon coupling in a magnetically frustrated multiferroic crystal; $YMnO_3$. This is done using inelastic neutron scattering on two triple-axis spectrometers; RITA2 and EIGER, stationed at the neutron source SINQ, PSI, Switzerland. Resent research has showed anomalous shifts in thermal conductivity (κ), magnetic susceptibility (χ) and heat capacity (C), as the $YMnO_3$ crystal undergoes an antiferromagnetic phase transition at its magnetic phase transition temperature, T_N. This behaviour can be understood as critical spin scattering of phonons in the phase transition region [3]. Our experiments show an avoided crossing of the phonon and magnon branch in our crystal, aswell as a shift in phonon width around the avoided crossing point, and around the magnetic phase transition.

Resume

I denne rapport har vi undersøgt hypotesen om phonon-magnon kobling i det magnetisk frustreret multiferroiske materiale; $YMnO_3$. Dette har vi gjort ved at anvende uelastisk neutron spredning på to triple-akse spektrometre; RITA2 og EIGER, lokaliseret ved neutronkilden SINQ, PSI, Schweiz. Den seneste forskning har vist kraftige ændringer i specifik varmeledningsevne (κ), magnetisk susceptibilitet (χ) og varmekapacitet (C), når $YMnO_3$ gennemgår en antiferromagnetisk overgang ved dens magnetiske faseovergangstemperatur, T_N. Denne opførsel kan forstås som kritisk spin spredning af phononerne ved den kritiske faseovergang [3]. Vores eksperiment viser at phonon- og magnongrenene undgår at krydse hinanden, samt en ændring i phonon bredden omkring dette krydspunkt, og omkring den magnetiske faseovergang.

1 Introduction

1.1 Motivation

Since the discovery of superconductivity, there has been considerations about its coupling to magnetism. This means that there have been reflections on whether ferroelectricity and ferromagnetism, which we will discuss later, are coupled or not. If there is such coupling, an exploitation of these electric-magnetic dynamics could bring a technological advance in creating/investigating superconducting materials, aswell as advance computer bit technology[2].

1.2 Magnetism and Ferroic properties

To describe magnetism in a material, we consider electron orbits and spins as magnetic dipole moments. We identify these magnetic moments as magnetic spins. Given a system with no external field applied above at high temperatures, the sum of the magnetic spins will equal zero over a statistical average of the magnetic spin vectors. We say that the system possesses complete rotational symmetry. However, if the system is cooled below the magnetic transition temperature, often refered to as the critical temperature, the magnetic spins will align themselves in some order [1]. This yields a broken symmetry of the system and therefore magnetic polarization, even when there is no external fields applied to the system. In the case where all magnetic spins point in the same direction, we call the system ferromagnetic, and the case where nearest-neighbour magnetic spin point in opposite direction, the system is called antiferromagnetic [[1],p92].

1.3 Multiferroiticity

A ferroic property describes changes in the physcial properties of a material as it undergoes a phase transition around a critical temperature. An example of this is the ferromagnet which shows a spontaneous magnetization below the critical temperature. As mentioned previously, ferroic properties are closely related to the symmetry of a given system. When the symmetry is broken we are able to define an order parameter, which displays the magnitude of the ferroic order. We can classify the known ferroic properties by considering symmetry under space-time inversion [2], and will be discussed later in Section 2.2. A table of the ferroic properties under space-time inversions are listed in Tabel 2.1.

1.4 Our experiment

We have investigated a rare-earth manganite, $YMnO_3$, which exhibits an exciting coupling between its structural and magnetic symmetries. It has been discovered that the manganite-ions in this crystal change their relative position in the crystal with up to 3% of the lattice constant, which is an enormous strain, below the magnetic phase transition temperature, $T_N \sim 70$K [3]. Research also shows anomalous behaviour of this crystals heatcapacity from around the magnetic phase transition temperature, T_N, to even (~ 200K) [4]. This leads to a hypothesis of a second interesting behaviour; temperature dependent coupling between spinwaves (magnons) and lattice vibrations (phonons) [4]. In this thesis we wish to examine this hypothesis using inelastic neutron scattering.

2 Magnetism and Multiferroicity

In this section we will describe the essential theory of magnetism and ferroic properties. In this context, we will discuss magnetic frustration and multiferroicity.

2.1 Magnetism

In the following subsections we will begin to describe general magnetism theory, starting with a brief summary of quantum mechanics.

In general, magnetic polarization and magnetization in matter arises from dipole moments at the nucleus, the moment from the electron orbits around the nuclei ($\mathbf{L}$), and a moment from the electron spin ($\mathbf{S}$). It is convenient to define the quantum number $\mathbf{J} = \mathbf{L} + \mathbf{S}$, which simplifies quantum mechanical calculations. In solids, nucleis and electrons are closely packed. This leads to interactions between the electrons which can induce different magnetic orders.
From quantum mechanics we know that in a simple case of two electrons, a and b, at positions $\mathbf{r}_1$ and $\mathbf{r}_2$, with corresponding states $\psi_a(\mathbf{r}_1)$ and $\psi_b(\mathbf{r}_2)$, they must have their joint wavefunction $\Psi = \psi_a(\mathbf{r}_1)\psi_b(\mathbf{r}_2)$ to be overall antisymmetric. We can write the overall wavefunction as a sum of a spatial part and a spin part. In the case of a symmetric spatial part, the spin part must be antisymmetric, and is called the *Singlet state*. In the opposite case where we have a antisymmetric spatial part, but symmetric spin part, the state is called the *Triplet state* [[1],p75]. We write the states as

$$\Psi_S = \frac{1}{\sqrt{2}}[\psi_a(\mathbf{r}_1)\psi_b(\mathbf{r}_2) + \psi_a(\mathbf{r}_2)\psi_b(\mathbf{r}_1)]\chi_S \tag{2.1}$$

$$\Psi_T = \frac{1}{\sqrt{2}}[\psi_a(\mathbf{r}_1)\psi_b(\mathbf{r}_2) - \psi_a(\mathbf{r}_2)\psi_b(\mathbf{r}_1)]\chi_T \ , \tag{2.2}$$

where χ_S and χ_T are the spin functions [[1],p14].
These states will have different energy levels, which we will denote E_S and E_T. By considering the difference between these energies we can define a quantity, J, entitled the *exchange constant* defined by

$$J \equiv \frac{E_S - E_T}{2} \ , \qquad \text{(Not to be confused with } \mathbf{J}\text{)} \tag{2.3}$$

The energies can be understood as spin interactions under the Heisenberg model, $\hat{\mathcal{H}}_{\mathrm{H}}$

$$\hat{\mathcal{H}}_{\mathrm{H}} = -2J\mathbf{S}_1 \cdot \mathbf{S}_2 \tag{2.4}$$

Nature strives for the lowest possible energy, so by considering the sign of J we are able to determine whether the singlet or triplet state is favoured. If $J > 0 \Rightarrow E_S > E_T$, and the triplet state is favoured. If $J < 0 \Rightarrow E_S < E_T$, and the singlet state is favoured[[1],p75].

2.1.1 Ferromagnetism

If $J > 0$ for all pairs of spins in our material, we will have a ferromagnetic material. A ferromagnet is a material which can induce a spontaneous magnetization, even without an applied magnetic field, below a certain temperature. One will find all the magnetic moments to be aligned along a single unique direction in the material [[1],p87]. We describe our spin system under the Heisenberg model as the spin-dependent part of our hamiltonian $-\sum_{ij} J_{ij}\mathbf{S}_i \cdot \mathbf{S}_j$, where J_{ij} is the exchange constant between the i^{th} and j^{th} spin. Considering a ferromagnetic material placed in a magnetic field $\mathbf{B}$, the Hamiltonian expands to

$$\hat{\mathcal{H}} = -\sum_{ij} J_{ij}\mathbf{S}_i \cdot \mathbf{S}_j + g\mu_B \sum_j \mathbf{S}_j \cdot \mathbf{B} \ , \tag{2.5}$$

where we recognize the last term as the Zeeman term.
To solve this Hamiltonian, it is necessary to do an approximation. We assume that all magnetic spins within the material feel the same magnetic field. This is commonly known as the *mean field approximation*. Under this approximation the Hamiltonian for our spin system can be written as

$$\hat{\mathcal{H}} = g\mu_B \sum_i \mathbf{S}_i \cdot (\mathbf{B} + \mathbf{B}_{\mathrm{mf}}) \ , \tag{2.6}$$

where $\mathbf{B}_{\text{mf}}$ is the mean field

$$\mathbf{B}_{\text{mf}} = \frac{2}{g\mu_B} \sum_{ij} J_i j \langle S_j \rangle = \lambda M \ . \tag{2.7}$$

$\langle S_j \rangle$ is the mean of the j^{th} spin, and λ is a constant.
We notice from equation 2.6 that even if $\mathbf{B} = 0$, the mean field $\mathbf{B}_{\text{mf}}$, which can be interpretered as a molecular field which interacts equally with all magnetic spins in the material, will render the hamiltonian nonzero. This leads to the ferromagnetic property; below a critical temperature (T_C), the magnetic spins will polarize and therefore magnetize the material. This spontaneous magnetization is the characteristic of ferromagnetism, where the magnetization of the ferromagnet can be used as an order parameter for the system [[1],p87].

2.1.2 Antiferromagnetism

If the coupling constant is negative for all pairs of spin in the material, $J < 0$, the magnetic spins align themselves antiparallel with respect to nearest-neighbour moments. This is called antiferromagnetism. We can evaluate an antiferromagnetic environment as being the sum of two sublattices; one sublattice containing all the 'up's (+), and one sublattice containing all the 'down's(−)[[1],p92], see Figure 2.1.

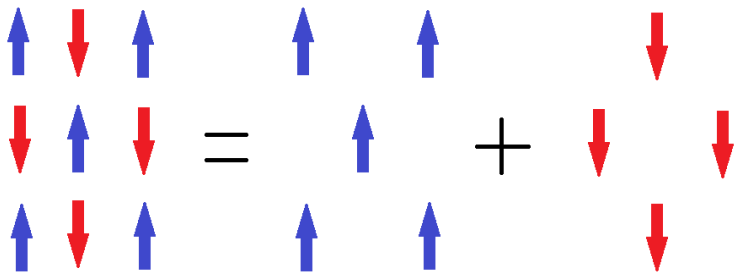

Figur 2.1: Breaking an antiferromagnet lattice into two sublattices.

We assume that the molecular field on one sublattice to be proportional to the magnetization of the other sublattice, and there are no external fields applied, and we are then able to describe the antiferromagnet under the Weiss model [[1],p92].

$$B_+ = -|\lambda| M_- \qquad , \qquad B_- = -|\lambda| M_+ \ ,$$

where λ is a constant which illustrates the strength of the molecular field. Since we have en equal number of magnetic spins pointing up and down the magnitude of the magnetization of the two sublattices are equal, hence we are able to write

$$|M_+| = |M_-| = M \tag{2.8}$$

While the net magnetization of an antiferromagnet is zero, due to the fact that the magnetization of the two sublattices are of equal magnitude and opposite direction, the difference $(M_+ - M_-)$ of the magnetizations will be non-zero (for $T < T_N$). This difference can be used as an order parameter for antiferromagnets [[1],p93].
As in ferromagnetism, the magnetic spin order will disappear above some critical temperature. The critical temperature for an antiferromagnet is called the *Néel Temperature*, T_N, and can be found experimentally which we will see later in Section 7

2.1.3 Magnetic Frustration

As we know from quantum mechanics, it is not always possible to find a unique ground state. This also applies for magnetic spins in a lattice. The lattice geometry can degenerate the energy levels of the system such that there will be an array of low energy states. There will be a large degree of 'non-energy minimization' shared across the low energy states, whereas the system will have a high level of ground state degeneracy. The system is said to be *geometrically frustrated* [[1],p165]. We consider an antiferromagnetic alignment of two different lattices under the Ising model (the spins may only be up (↑) or down (↓)). The lattice in Figure 2.2 is able to align all of its magnetic spins antiferromagnetically, and therefore the energy between nearest-neighbor interactions are minimized. Looking at Figure 2.3. The two magnetic spins at the bottom of the figure have aligned themselves antiferromagnetically, and their interaction energy is minimized. Now, as we try place the 3$^{\text{rd}}$ magnetic spin, we are not able to satisfy antiferromagnetic alignment for the whole system. Two of the magnetic spins will be aligned parallel, and the other antiparallel. There will be no energy difference in the system from having two 'downs' and one 'up', or having one 'down' and two 'ups'. The energy ground state is degenerate and we can therefore classify our system as *frustrated*[[1],p.165].

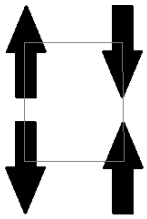

Figur 2.2: Antiferromagnetic alignment on a square lattice.

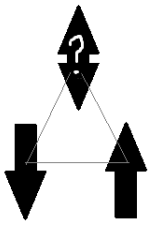

Figur 2.3: Antiferromagnetic alignment on a triangular lattice. The system is frustrated.

Note that due to the high degeneracy of energy levels in a frustrated magnet the system is metastable and will therefore have a time-dependent relaxation towards equilibrium [[1],p166].
In order to classify how frustrated a magnet is, we calculate the *frustration index*, which is defined as [3]

$$f = \frac{|\theta_{CW}|}{T_N} \tag{2.9}$$

, where θ_{CW} is the Curie-Weiss temperature (We have a spontaneous magnetization at and below this temperature [5]).

2.2 Multiferroics

Earlier we discussed the ferroic property, ferromagnetism. We saw that this ferroic property can be described using order parameters. Order parameters can be used to describe the mutual magnetization, polarization, and/or strain of the ferroic material. By considering space-time symmetry under inversion, the four ferroic properties of matter can be categorized as in Table 2.1:

	Space invariant	Space variant
Time invariant	Ferroelastic	Ferroelectric
Time variant	Ferromagnetic	Ferrotoroidic

Tabel 2.1: Multiferroic properties and their symmetries under space-time inversion.

A material which possess two, or more, of these ferroic properties is said to be a *multiferroic* [2].

Furthermore, research in multiferroics has expanded to include antiferroic symmetries, such as antiferromagnetism.
The ferromagnetic and ferroelectric properties have been a hot topic in research the latter years. Eerenstein et al. [2] write that they couple, through the *magnetoelectric* coupling. This magnetoelectric coupling may appear directly between the two order parameters or indirectly via strain.[2]. It has been suggested it would be possbile to create 4-state memory with magnetoelectric coupling, or even be able to write data using electric signals and read it magnetically [2]. To understand magnetoelectric coupling we will consider the three parameters, electric polarization (**P**), the magnetization (**M**), and strain (ε). We assume that we have a ferro-electric/magnetic multiferroic material. According to Table 2.1, the material will have a spatial invariant, time variant order parameter (ferromagnetism), and a spatial variant, time invariant order parameter (ferroelectricity). In total the multiferroic material which carries both the ferroelectric and ferromagnetic order parameters, will have its symmetries compromised, and neither possess spatial nor time symmetry [2]. This asymmetry is visualized in Figure 2.4

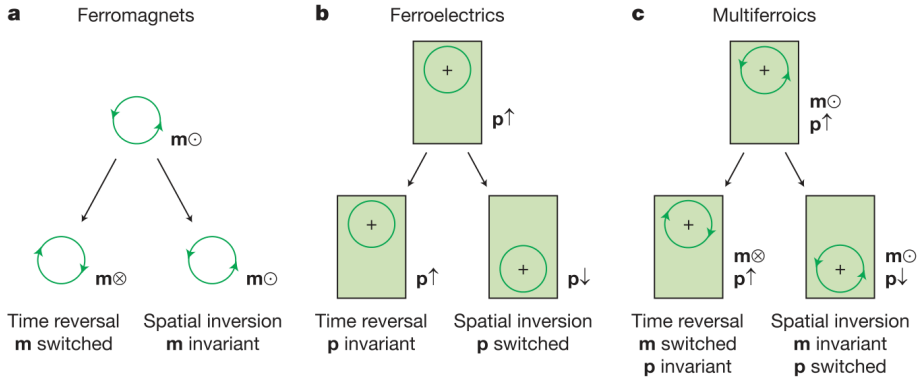

Figur 2.4: Space-time inversion symmetry in ferroics and multiferroics. **a**) We see the time asymmetry of ferromagnetism. **b**) The spatial asymmetry of ferroelectricity. **c**) The multiferroic with both ferroelectricity and ferromagnetism possess no symmetry under the space-time inversion. Picture taken from Eerenstein et al. [2].

We draw the following relations:

- (**a**) Ferromagnet. The local magnetic moment (**m**), induced by a charge moving in a loop varies in time. As we make a time reversal, the charge will move in the opposite direction, thus the induced magnetic moment will point in the opposite direction.
- (**b**) Ferroelectric. The local dipole moment (**p**) is shown as a positive pointcharge. The charge will not change under time reversal, but as we make a spatial inversion (mirror the system around its symmetry-axis) the charge is displaced, thus variant under spatial inversion.
- (**c**) Multiferroic. A multiferroic that is both ferromagnetic and ferroelectric does not posses symmetry under space-time inversion.

According to Eerenstein et al. [2], we are able to exemplify our magnetoelectric coupling as the following. Theoretically we can describe the magnetoelectric coupling using Landau theory; Taylor expansion of the order parameters. We write the free energy F in terms of the electric field $\mathbf{E}(T)$, and the magnetic field $\mathbf{H}(T)$ [2]. For simplicity we assume a material non-ferroic, infinite, homogeneous, and stress-free. We can then write the free energy (F) as the following

$$-F(\mathbf{E},\mathbf{H}) = \frac{1}{2}\epsilon_0\epsilon_{ij}E_iE_j + \frac{1}{2}\mu_0\mu_{ij}H_iH_j + \alpha_{ij}E_iH_j + \frac{\beta_{ijk}}{2}E_iH_jH_k + \frac{\gamma_{ijk}}{2}H_iE_jE_k + \dots \quad (2.10)$$

The first two terms shows the systems electric/magnetic response to an electric/magnetic field. The third term shows the linear magnetoelectric coupling with coupling constant $\alpha_{ij}(T)$, and the

last terms represent higher-order magnetoelectric couplings.
We can obtain the electric polarization of our magnetoelectric system by differentiating eq(2.10) with respect to E_i, and setting $E_i = 0$. To obtain the magnetization, we can evaluate similarly with H_i. This yields the two expressions below

$$P_i = \alpha_{ij} H_j + \frac{\beta_{ijk}}{2} H_j H_k + \dots \ , \qquad \mu_0 M_i = \alpha_{ji} E_j + \frac{\gamma_{ijk}}{2} E_j E_k \dots \tag{2.11}$$

Recall that this computation was done for non-ferroic materials, but will look somewhat alike for a ferroic material, but with a more complicated parametrization [2]. Eq(2.11) shows explicit that the magnetoelectric coupling motivates for a connection between the electric polarization of a material and the magnetic fields, and the magnetization of the material and the electric fields [2].

3 Phonons and Magnons

In this section we will describe lattice and spin excitations and their dispersion relations.
Lattice vibrations, phonons, are oscillations in the relative position of the ions on a lattice [5]. We can describe the ion displacements with respect to the lattice planes (s) in equilibrium with a single coordinate (u_s). Assuming that the elastic response of the crystal is a linear function of the displacements we can write the force as a form of Hooke's law [5].

$$F = C\left((u_{s+1} - u_s) + (u_{s-1} - u_s)\right) \ , \tag{3.1}$$

where C is the force constant between nearest-neighbour planes.
Treating our problem as a classical harmonic oscillator, we can derive the dispersion relation of the (phonons) as the following

$$\omega^2 = \frac{2C}{M} \cdot (1 - \cos(\mathbf{k}a) \ , \tag{3.2}$$

where C is the force constant, M is the mass of the vibrating ions, $\mathbf{k}$ is the wave vector, and a is the lattice constant. The lattice vibration dispersion relation is shown in Figure 3.1.
Spin waves, magnons, are oscillations in the relative orientation of spins on a lattice [5]. The oscillations can be described as spin precessions with a constant angle. Considering the spins as classical vectors and their nearest-neighbour interactions under the Heisenberg model, eq(2.4), we are able to make a classical derivation of the magnon dispersion relation [5].

$$\hbar\omega = 4J \cdot S\left(1 - \cos(ka)\right) \ , \tag{3.3}$$

where J is the exchange constant, S is the spin, k is the wavenumber, and a is the lattice constant. The spin wave dispersion relation is shown in Figure 3.1.

4 Neutron Scattering

Neutron scattering is a widely used experimental technique to determine structural and physcial dynamics of materials down to the atomic scale. In the following we will go through essentiel theory behind neutron scattering and instrumentations.

4.1 The Neutron

Neutrons interact with nuclei through the strong nuclear force, and with magnetic spins through the electromagnetic force. The neutron is an eletrically neutral, spin $s = 1/2$, particle with mass

$$m_{\mathrm{n}} = 1.675 \cdot 10^{-27}\mathrm{kg} \tag{4.1}$$

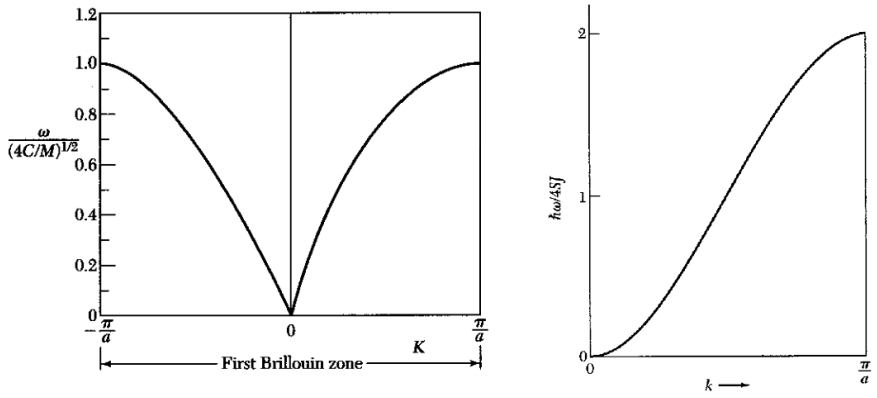

Figur 3.1: (right) Dispersion relation for phonons in the 1st Brillouin zone. (left) Dispersion relation for magnons in a ferromagnet. Pictures taken from Kittel [5].

The neutron has an average lifetime of $\tau = 886$s, before it decays into a proton, electron, and an anti-neutrino. Neutron decay can be neglected in neutron scattering, since the lifetime is much longer than the time spend on the actual experiment.
A neutron posses a magnetic moment, which is coupled antiparallel to its spin in the order of

$$\mu = \gamma \mu_{\mathrm{N}} \ , \tag{4.2}$$

where $\gamma = -1.913$ is the neutron gyromagnetic ratio, and μ_{N} is the nuclear magneton given by $\mu_{\mathrm{N}} = e\hbar/m_{\mathrm{p}} = 5.051 \cdot 10^{-27}\mathrm{J/T}$.
Thus we are dealing with physics on the atomic scale, and thus we must account for quantum mechanical effects. The first thing to consider is the particle-wave duality. Neutrons displays shifting particle-wave properties throughout a neutron scattering experiment. As the neutrons are created in a source, they are considered as particles. Then, at the sample where the neutrons are scattered, the neutrons behave as interfering waves, and again considered as particles when they are detected.
When dealing with particle-wave duality, we consider the wavelength, λ, of a particle moving with constant velocity, v, as

$$\lambda = \frac{2\pi\hbar}{mv} \tag{4.3}$$

When doing neutron scattering the wave nature of the neutrons are often refered to as the *wave vector*, which is defined as

$$\mathbf{k} = \frac{m_{\mathrm{n}}\mathbf{v}}{\hbar} \tag{4.4}$$

The velocity of the neutrons are usually small (compared the speed of light) so we consider the neutrons as being non-relativistic, and we can then write the neutron kinetic energy as

$$E = \frac{\hbar^2 k^2}{2m_{\mathrm{n}}} \tag{4.5}$$

By tradition, wavelenghts are measured in Å(10^{-10})m, wavenumber is measured in Å^{-1}, velocity is measured in m/s, and energy is measured in eV or meV.

4.2 Scattering

In this section we will go through the most central equations of scattering. First we will have a quick walkthrough of the scattering cross section. Many of the quantities used in this walkthrough will be discussed in the following subsections

4.2.1 Scattering cross section

The scattering cross section (σ), is somewhat proportional to [12]

$$\frac{\partial^2\sigma}{\partial\epsilon\partial\Omega} \propto \sum_j e^{iqr_j} \ , \tag{4.6}$$

where ϵ is the neutron energy after scattering, Ω is the solid angle, q is the scattering vector and r_j is the j^{th} positionvector in the lattice.
In an infinite lattice we will have an infinite amount of r_j, we know from Euler mathematics that an exponential function of this form is an periodic function with values on the unit circle. The sum of infinite random points on the unit cirlce will equal zero. If the sum equals zero, we have no scattering cross section, and we will not see anything when measuring. But if we define our scattering vector as $q = \frac{2\pi}{r_j}$, the sum will be nonzero, since $e^{2\pi i} = 1$. We notice that q is given by 2π divided by a charaterisctic lattice vector, which we recognize as a reciprocal lattice vector for a square lattice. It is therefore convenient to work in reciprocal space when doing neutron scattering.

4.2.2 Scattering (continued)

The foremost important vector in scattering is the *scattering vector*, $\mathbf{q}$ (see Figure 4.2), defined as

$$\mathbf{q} = \mathbf{k}_i - \mathbf{k}_f \ , \tag{4.7}$$

where $\mathbf{k}_i$ denotes the incoming wave vector, and $\mathbf{k}_f$ denotes the outgoing wavevector, see Figure 4.2.
A central equation when doing elastic scattering ($|\mathbf{k}_i| = |\mathbf{k}_f|$) is the famous Braggs law for diffraction

$$n\lambda = 2d \cdot \sin(2\theta) \tag{4.8}$$

, where d is the lattice spacing, n is an integer, and θ is the scattering angle.
This equation shows that it is necessary to know the wavelength of the incoming neutrons. The determination of the neutron wavelength can be done by two methods which selects a particular energy spectra of neutrons. The most efficient of these is to use a *monochromator*, which is a crystal that only reflects neutrons of certain wavelengths using Bragg reflection. The monochromator reflects a series of wavelength of integer n, where $n = 1$ usually is the desired neutron wavelength for the experiment, and the higher order wavelengths are undesired. We are able to extinguish the amount of higher order wavelengths using filters and/or neutron guide geometry.
Some scattering processes can absorb or transfer energy to the scattering system. This type of scattering is refered to as *inelastic neutron scattering*. In this case $|\mathbf{k}_i| \neq |\mathbf{k}_f|$, due to the energy transfer to the scattering system. We define the energy difference as

$$\hbar\omega = E_i - E_f = \frac{\hbar^2(k_i^2 - k_f^2)}{2m_{\text{n}}} \tag{4.9}$$

Now that we have introduced neutron theory we will move on the the instruments used during neutron scattering.

4.3 Triple-Axis Spectrometer (TAS)

In this thesis we have made inelastic neutron scattering in order to examine the $YMnO_3$ crystal. As shown in eq(4.9), it is necessary to determine both k_i, and k_f, in order to calculate the energy difference from the inelastic collisions. When using a *triple-axis spectrometer (TAS)*, Figure 4.1, these quantities can be selected, and held constant, using neutron monochromators and Bragg

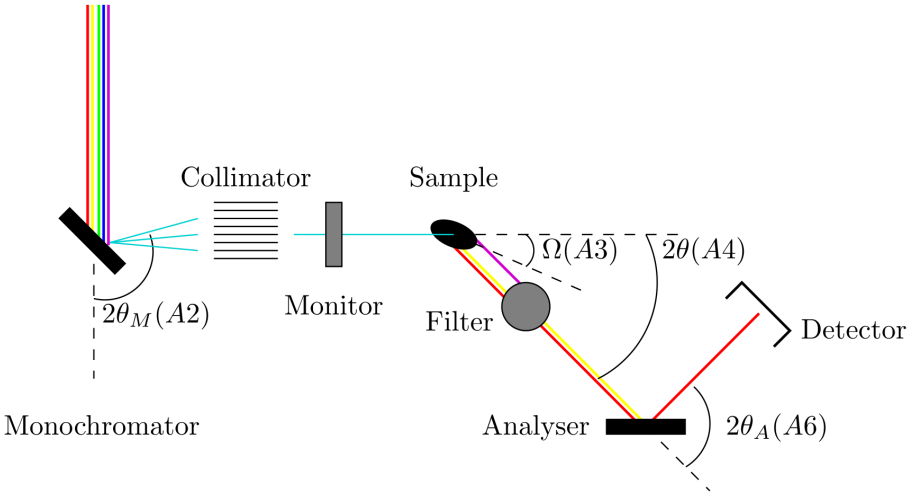

Figur 4.1: Sketch of a typical triple-axis spectrometer (TAS). The three scattering angle; $2\theta_m$, 2θ, $2\theta_a$ and the sample rotation Ω is shown. Figure taken from neutron scattering notes [12].

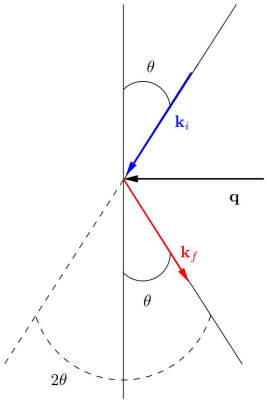

Figur 4.2: Wave vector $\mathbf{q}$.

reflections eq(4.8).
Note that the name *triple-axis spectrometer*, is due to the fact that the neutrons are scattered three times before they reach the detector. The three scattering objects are:

- A MONOCHROMATOR, which selects k_i from the incoming beam by the Bragg scattering angle $2\theta_M$ eq(4.8).
- The SAMPLE, which scatters the monochromatic beam by 2θ.
- An ANALYSER, which determines k_f likewise as for the monochromator. It scatters with an angle $2\theta_A$ determined by Braggs law eq(4.8).

Additionally we have three devices to count, filter, or focus the beam:

- A COLLIMATOR is an object with typically $\sim$ 1m long, thin parallel neutron-absorbing planes, which reduces the divergence of the incoming neutrons.
- A MONITOR, which lies perpendicular to the incident beam. This device count an amount of neutrons pr. perpendicular unit area, also known as Flux (Ψ).
- A FILTER, which suppresses undesired higher-order wavelengths.

By adjusting these angles and the sample rotation, Ω, we can obtain a wide extent of scattering vectors $\mathbf{q}$, and energy transfer $\hbar\omega$ which satisfies the scattering condition eq(4.7). When doing TAS experiments an experimental series consist of *scans* along a certain axis in the $(\mathbf{q}, \hbar\omega)$-space, often refered to as constant-q scans or constant-energy scans, depending on which variable is fixed throughout the scan.
Notice that the different scattering angles and/or instrument parameters on a triple-axis spectrometer is named as A1 - A6. This is common neutron scattering jargon identifying the instrument parameters, and will be used throughout the thesis. The A's are listed below

- A1 - Denotes the rotation of the monochromator.
- A2 - Denotes the scattering angle on the monochromator ($2\theta_M$).
- A3 - Denotes the sample rotation (Ω).

- A4 - Denotes the scattering angle on the sample (2θ).
- A5 - Denotes the rotation of the analyzer.
- A6 - Denotes the scattering angle on the analyzer ($2\theta_A$)

Additionally it is common to fix either E_i or E_f in order to simplify the data analysis of the measurements.

5 Instruments and Sample

In this section we will discuss the two triple-axis spectrometers used for our experiments and their differences. Our $YMnO_3$ sample will also be presented.
Two instruments where used in order to complete this project. This is due to a difference in spectrometer scan range, and neutron source energy. When doing neutron scattering the following neutron sources are used

Energy Interval	λ interval	Source Name
(0.05 - 14)[meV]	(2.4 - 40)[Å]	cold
(14 - 200)[meV]	(0.6 - 2.4)[Å]	thermal

Tabel 5.1: Table of common energies, and name for neutron sources. Values taken from neutron course notes [12].

The two triple-axis spectrometer that we used are both located at the Paul-Scherrer Institute (PSI), Switzerland. Both are located at the SINQ continuous spallation source, with a neutron flux of $\sim 3 \cdot 10^{13}$[n/cm^{2}s][17].

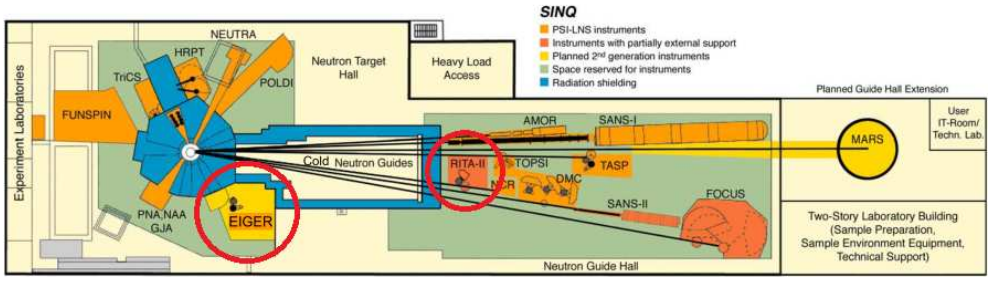

Figur 5.1: Picture of SINQ neutron source at PSI, Switzerland. The two instruments, EIGER and RITA, are marked with a red ring. Picture taken from PSI powerpoint presentation [17]

5.1 EIGER

EIGER is a triple-axis spectrometer located at the SINQ neutron spallation source at PSI, Switzerland. The spectrometer is placed at a thermal neutron source, see Table 5.1 for neutron parameters. As we see in Figure 5.1, EIGER is located close the neutron source. This results in a high neutron flux for the incident neutron beam, in addition to a large energy range due to the use of thermal neutrons.
The instrument setup is, as following the beam progression: First, the thermal neutrons scatters on the monochromator on the $(h\ k\ l) = (0\ 0\ 4)$ Bragg reflection. The monochromator is a pyrolytic (PG) crystal consisting of 9×15 square tubes, which are 2×2[mm^2] wide. Then the beam is focused through a collimator and send through slit1 (see Table 5.2). Next the beam is scattered on our sample, send through slit2 (see Table 5.2), and a 37[mm] PG filter. Here the beam is scattered on the $(h\ k\ l) = (0\ 0\ 4)$ Bragg reflection on the analyser. Also a PG crystal. Last the beam goes through slit3 (see Table 5.2), and is observed in the detector.

Tabel 5.2: Slit openings on EIGER.

Units = [mm]	Slit 1	Slit 2	Slit 3
Horizontal	25	25	20
Vertical	60	30	60

5.2 RITA2

The RITA2 instrument is a multi-analyzer TAS at the SINQ spallation neutron source at PSI, Switzerland, see Figure 5.1. The instrument is placed at a cold neutron source, see Table 5.1 for neutron parameters.
RITA2 has, in contrast to other triple-axis spectrometers, nine PG analyzer blades after the sample. This design yields a greater efficiency of the incident neutron beam, since the instrument will look at nine points in **q**-space simultaneously.
The instrument setup is, as following the beam progression: As the neutrons leave the source they are guided to a monochromator consisting of five pyrolytic graphite (PG) crystals. Then, the neutrons pass through a 80' collimator. The sample can be placed in a cryostat, which can cool down to 1.6K. After the sample, an optional Be-filter is placed to remove undesired higher-order wavelengths.
With RITA2's nine analyzer blades, we are scanning nine points in the $(\mathbf{q}, \hbar\omega)$-space simultaneously when we sample our data. Since the blades are not perfectly identical, there will be a variance in neutron intensity over the blades as we scan. Therefore we need to normalize the blades with respect to each other to be able to evaluate the collected data equally. This is done by marking an area around for each analyzer blade on an intensity plot, Figure C.1. Each blade intensity is then divided by the intensity of the middle blade, the 5th blade, thus making the 5th blade our reference blade, see Table 5.3.
The normalization of intensity on the nine RITA2 blades yields the following factors on the nine blades

Tabel 5.3: Normalization values of RITA2's nine blades.

Blade nr.	1	2	3	4	5	6	7	8	9
	0.686	1.036	0.879	0.992	1.000	0.830	0.810	0.710	0.664

When doing our data analysis on the RITA2 data, we must account for the relative positions of the nine analyzer blade aswell. This means that we need to make a projection of the scans done in q-space onto one of the $(h\ k\ l)$-axes in order to visualize our data.

5.3 The $YMnO_3$ Crystal

Now we will discuss the $YMnO_3$ crystal used for experiments, describing its lattice parameters and physical properties. The rare-earth manganite $YMnO_3$ is a highly-frustrated multiferroic sytem, which exhibits a strong coupling between the magnetic moments, and the ion positions on the lattice. We therefore also have a coupling between the magnetic excitations and the phonon modes [3]. Below the antiferroelectric transition temperature, $YMnO_3$ crystallizes in a hexagonal structure arranging its Mn^{3++}-ions, which are coupled antiferromagnetically, in triangular networks in $c = 0$, and $c = 1/2$ layers. These layers form ABAB stacking along the c-axis, see Figure 5.2, where the Mn^{3++}-ions bindings to the Y- and O-ions results in large separation of the manganite ions [10].
The crystal has lattice constants $a = b = 6.140$Åand $c = 11.393$Å[10]. With angles $\alpha = \beta = 90°$ and $\gamma = 120°$. The thermal conductivity of $YMnO_3$ has been shown to be slightly suppressed in the region of the magnetic phase transition temperature, T_N, and even further (~ 200K), due to critical fluctuations of spins in the frustrated system. There has been observed anomalous changes

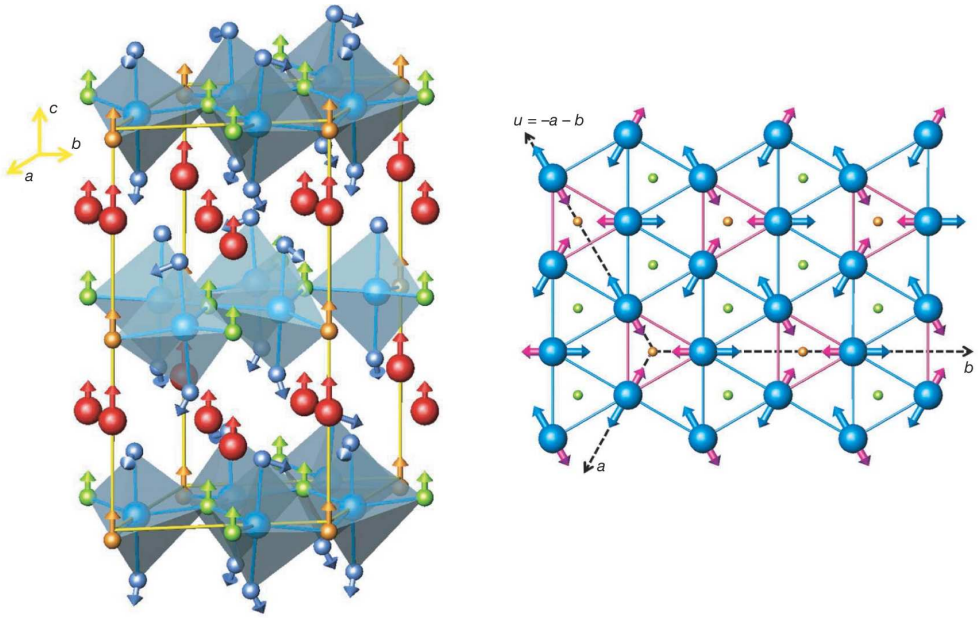

Figur 5.2: Red = Y, light blue = O, dark blue = Mn. (right) Unit cell of $YMnO_3$ hexagonal structure arrows shows dispalcement then below T_N. (left) Mn-ion displacements below T_N. Picture taken from Lee et al. [3].

in the magnetic susceptibility (χ), and heat capacity (C), for the $YMnO_3$ crystal aswell, shown in Figure 5.3 taken from Sharma et al.[4].

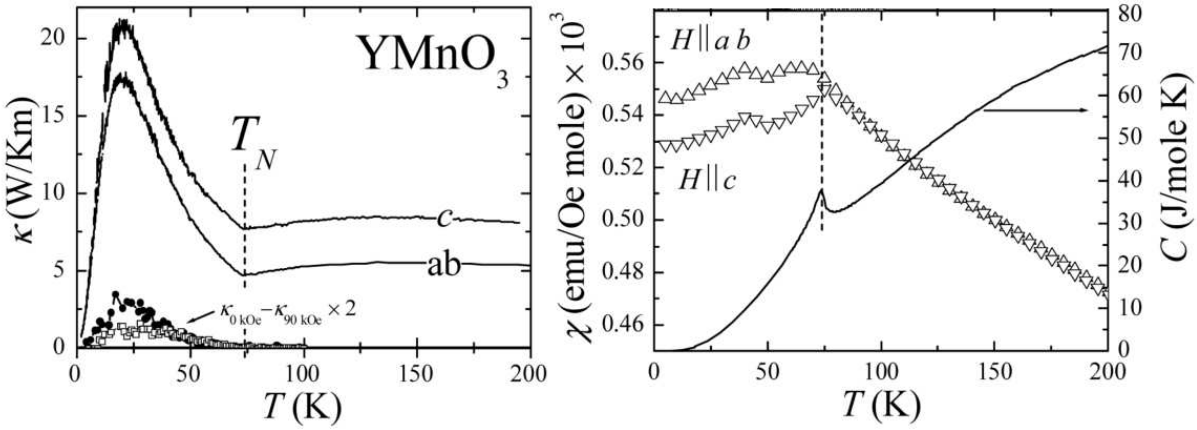

Figur 5.3: Thermal conductivity (κ), magnetic susceptibility (χ) and heat capacities (C) anomalies around T_N. Plots taken from Sharma et al.[4].

Sharma et al. also found a second transition in χ around 40K, which is assumed to be caused by spin reorientation of the Mn^{3++}-ions[4]. Evidently, a large Mn^{3++}-ion displacement has been observed around T_N for $YMnO_3$ by Lee et al. [3]. The shift in ion position of the manganite-ions have been recorded to lay around 3.3% off relative to the lattice constants. This shift is enormous compared to usual strain and leads to a further coupling to the electric dipole moments [3]. The shift in ion positions is a consequence of the the magnetic transition of the crystal. Therefore, the displacement is a coupling between the elasticity (strain) and antiferromagnetic. The displacements does also allow an antiferroelectric transition and hence we have antiferroelectric and antiferromagnetic coupling [3].

5.3.1 Sample

Our crystal is a 21.0mm long, with a diameter of 1.0cm, cylindrical $YMnO_3$ crystal. It has a mass of 5250mg. The initial alignment of the sample has been done using a X-Ray Laue camera. The sample is attached to a aluminium handle (no glue) . A picture of the sample is shown in Figure 5.4, where the black dot marks the (1 0 0) axis.

Figur 5.4: Picture of our sample. The black dot indicates the (1 0 0) axis.

6 Measurements

To study the phonon excitations in our crystal, we have used the EIGER TAS and scanned around the Bragg peak $q(h\ k\ l) = (0\ 3\ 0)$. On the RITA2 TAS, we have studied the magnetic excitations around the magnetic Bragg peak $q(h\ k\ l) = (0\ \ -1\ 0)$. Recall from Section 4 that we scan in $(\mathbf{q}, \hbar\omega)$-space, so I will use terms as 'Energy scans' and '$\mathbf{q}$ scans', which refers to which parameter is variated throughout the measurement.

6.1 EIGER data

On EIGER we measured longitudinal phonons. To measure a longitudinal phonon we must ensure that our $\mathbf{q}$-vector and the phonon is parallel to eachother [12], therefore we need to make transverse scans. Our crystal is a hexagonal environment and we must find the perpendicular (transverse) direction to our axes. Consider the triangle on Figure 6.1.

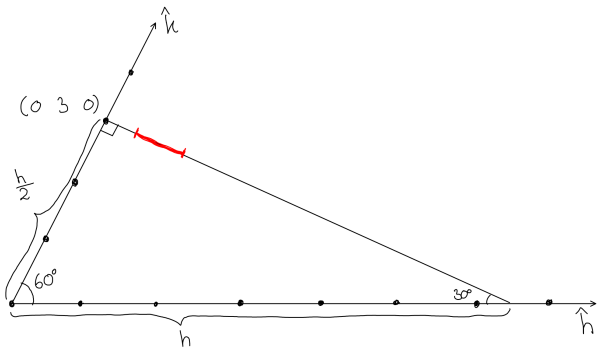

Figur 6.1: Drawing of trigonometric problem to make transverse scans. The red area indicates where we made our transverse phonon scans.

The $\hat{h}$ and $\hat{k}$ denotes the h- and k-axes in our hexagonal lattice. We have derived the $\frac{h}{2}$ side by calculating $\sin(30°) = \frac{h}{x} \rightarrow x = \frac{h}{2}$. The vector $h - \frac{h}{2}$ is perpendicular to the k-axis. We have now found the transverse direction and can thus define

$$q_{\text{trans}} = \begin{pmatrix} h & k - \frac{h}{2} & 0 \end{pmatrix} \tag{6.1}$$

Which will be the transverse direction at the wanted k value in our lattice.
We made energy scans along the transverse direction around $q(h\ k\ l) = (0\ 3\ 0)$, see the red line at Figure 6.1, in order to map the phonon at $T = 100$K and both phonon and magnon at $T = 40$K. Two of the raw data profiles are shown in Figure 6.2 and Figure 6.3 (the rest in Appendix A), the color maps are showed on Figure 6.4 and Figure 6.5.

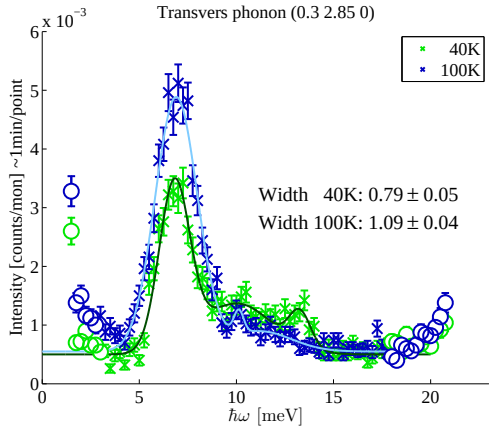

Figur 6.2: Phonon-Magnon peaks at 40K and 100K, $q \approx (0.3\ 2.85\ 0)$.

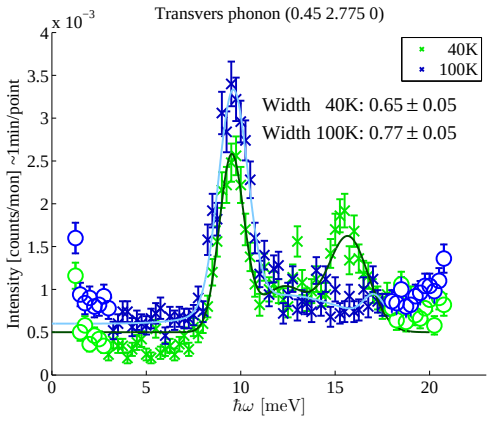

Figur 6.3: Phonon-Magnon Map at 40K and 100K, $q \approx (0.45\ 2.775\ 0)$.

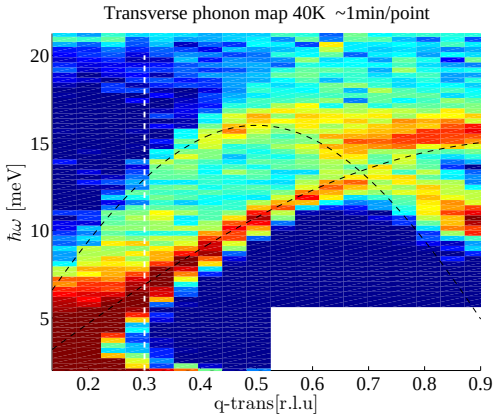

Figur 6.4: Phonon-Magnon Map at 40 K, $q \approx$ (0 3 0).

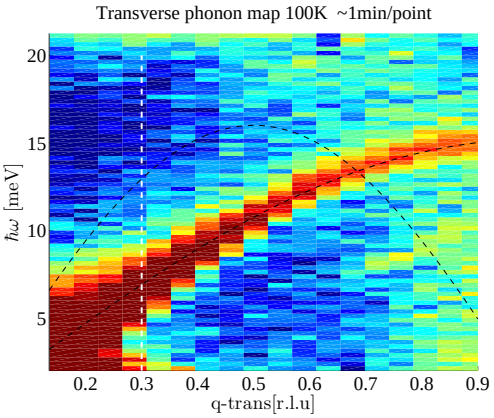

Figur 6.5: Phonon-Magnon Map at 100 K, $q \approx$ (0 3 0).

Dotted black lines are sinusoidal guidelines with integer periods. Dashed white lines indicates where we scanned in Figures in Appendix B.

Additionally we made a serie of energy scans around $q(h\ k\ l) = (0.35\ 2.825\ 0) \rightarrow |q| = 0.3$ (shown with a dashed white line in Figure 6.4 and Figure 6.5), at different temperatures. This was done in order to get a correlation between the phonon and magnon branches. These scans are shown in

Appendix B and evaluated under the discussion section.
We made a series of constant-**q** temperature scans around the $q(h\ k\ l) = (0.35\ 2.825\ 0)$ longitudinal phonon. The raw phonon peak profiles is a shown are Figure 6.6.

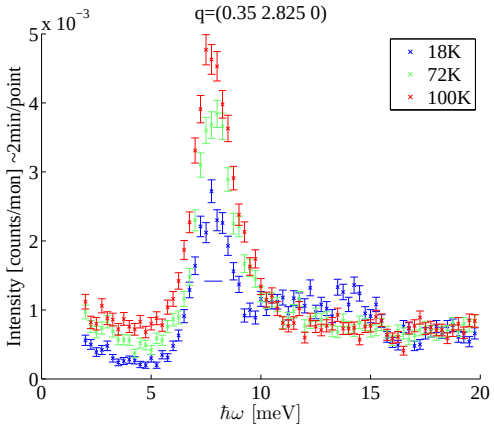

Figur 6.6: Phonon profiles at different temperatures around $|q| = 0.3$. The small blue horizontal bar is an estimate of the instrument resolution

The instrument resolution is estimated as the mean of the instrument resolution at the three different temperatures. When we are calculating the uncertainty of the widths of our peaks, the uncertainties are added quadrature as the following

$$(\sigma_{\text{obs}})^2 = (\sigma_{\text{res}})^2 + (\sigma_{\text{mea}})^2\ , \tag{6.2}$$

where σ_{obs} is the observed peak width, σ_{res} is the resolution contribution, and σ_{mea} is the uncertainty what we measure (in this case phonons). Thus the contribution from the instrument resolution is small and squared, we neglect any instrument resolution part in our data analysis.

6.2 RITA data

We made a serie elastic-**q** scans along l around $q(h\ k\ l) = (0\ -1\ 0)$ at different temperatures in order to investigate the magnetic phase transition. We aim to determine T_N and the critical exponent (2β). This will be evaluated under the discussion section and is shown in Figure 7.7.
An serie of (q_h, q_k) scans were made to map the $q(h\ k\ l) = (0\ -1\ 0)$ magnetic peak at five different temperatures. Two of these maps are shown in Figure 6.7 (the other maps can be found on Figure D.1 and D.2), notice that the magnetic peak has some anomalies on the edges. To check if these anomalies was a special case for the $(0\ -1\ 0)$ peak, we made a map of the $q(h\ k\ l) = (0.5\ -1\ 0)$ peak aswell, which shows same shape, see Figure D.2(right).
We also made energy scans of the $q(h\ k\ l) = (0\ -1\ 0)$ magnon at $T = 40$K which revealed a splitting of the spinwave excitations around this peak, see Figure 6.8
On Figure 6.8 we a splitting of the magnon branch around h[r.l.u] $= -1.1$. We made three scans along h[r.l.u] $= -1.1$, the dashed line in Figure 6.8, at $T = 18$K, $T = 40$K and $T = 60$K to find the temperature dependency of the spinwave. The profiles of the magnon peaks at these three temperatures is shown on Figure 6.9

7 Discussion

Our goal is to investigate suspected phonon-magnon coupling and to get a wider understanding of multiferroic behaviour. In order to investigate these subjects we must examine the magnetic order and behaviour of our $YMnO_3$ crystal and put it in perspective to our theory.

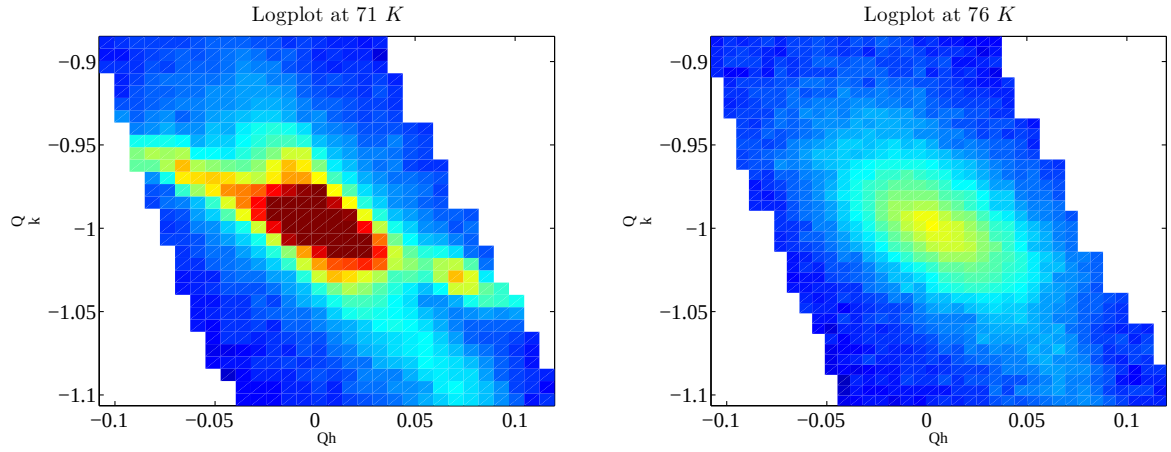

Figur 6.7: Bragg peaks at $q = (0\ -1\ 0)$.

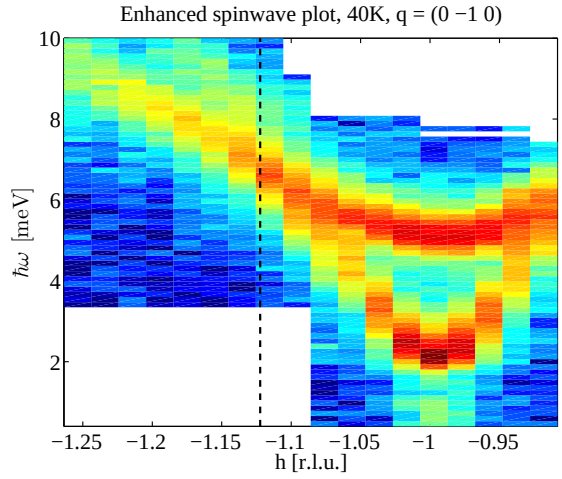

Figur 6.8: Spinwave splitting of magnon modes around $q = (0\ -1\ 0)$. The black dashed line shows where we scanned to make our peak profiles in Figure 6.9. Colour scale on plot has been reduced in order to enhance the branches the plot.

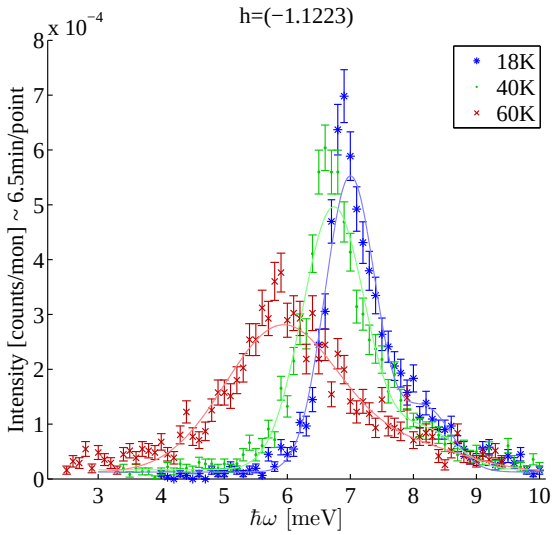

Figur 6.9: Raw magnon peaks at h[r.l.u] $= -1.1223$ on Figure 6.8.

7.1 Phonon-magnon coupling

We consider the two colormaps in Figure 6.4 and Figure 6.5. We notice the avoided crossing of the phonon-magnon branches around q[r.l.u] $= 0.7$. If phonons and magnons had no coupling, they would cross each other without being affected by one another. But as they close in on each other, the magnon branch seems to 'bounce off' while the phonon branch is bend down. This suggests for interactions between phonons and magnons in the solid. Also, there seems to be a slightly higher scattering intensity between the phonon-magnon branches, than above the magnon branch. This intensity shift could be sign of magnetoelectric coupling interactions, but we need further data and analysis to conclude anything. We made a number of gauss fits along each scan column to estimate the widths (σ) of the phonon and magnon excitations as the extend in **q**-space. In Figure 7.1 and Figure 7.3 we see a sudden shift in σ from $q_{\text{trans}} \approx 0.6$, for both the magnon and phonon, which is around the avoid crossing point. According to Lee et al. this shift can be understood as critical spin scattering of phonons [3]. This behaviour strongly indicate coupling between the phonon and magnon modes. Additionally we see that the shift of the phonon width has disappeared at high temperatures, see Figure 7.2.

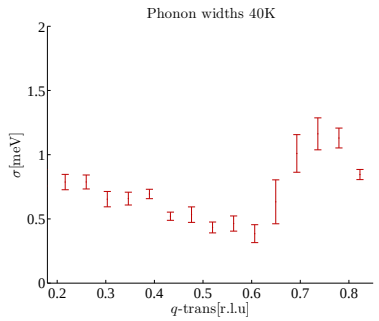

Figur 7.1: Width of phonon mode in Figure 6.4.

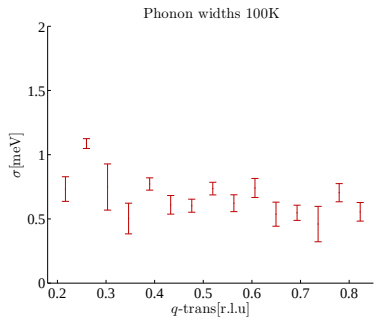

Figur 7.2: Width of phonon mode in Figure 6.5.

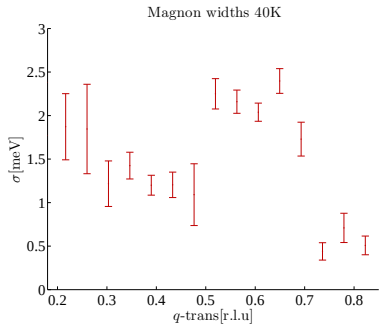

Figur 7.3: Width of magnon mode in Figure 6.4.

To process the relation of phonon-magnon widths we split up in each scan row of Figure 6.4 and 6.5 (the vertical rows), and fitted with a suiting number of gauss fits. By means of this, there have been accounted noise between the two branches. The first points in the phonon and magnon widths have been removed since that peak was to offset in our data to have a welldefined gauss fit, or because the magnon has not appeared yet.
As we described in the theory section, magnetic order, and therefore also magnetic excitations, is temperature dependent. Thus we assumed phonon-magnon coupling to be temperature dependent aswell, and made a series of transverse scans around the $q(h\ k\ l) = (0\ 3\ 0)$ phonon from 17.6K to 99.2K. The scan serie can be seen in AppendixA.
We plotted the widths, and integrated intensity, as a function of temperature and found the following results

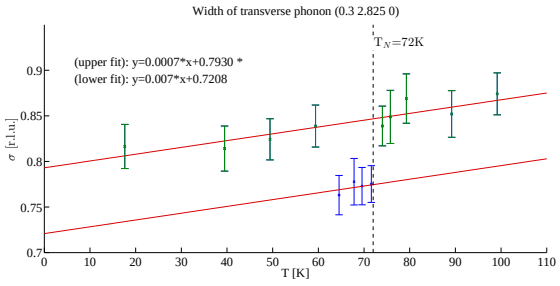

Figur 7.4: Temperature dependence of width for transverse phonon($q = (0.3\ 2.825\ 0)$). Fitted linearly with same slope. The lower fit has its slope locked to the slope of the upper.

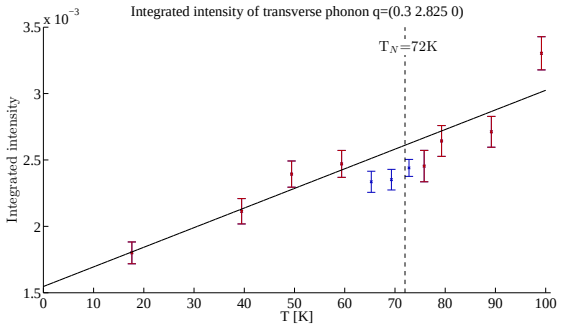

Figur 7.5: Temperature dependence of intensity for transverse phonon ($q = (0.3\ 2.825\ 0)$). Fitted to the bose-factor.

The blue points in both Figures shows the same interval just below T_N.

In figure 7.4, the slope of the lower fit is fixed to the slope of the upper in order to find the shift in phonon width, $\Delta\sigma$. From Heisenberg, we know that $\Delta E \Delta t \geq \hbar$. Recall from eq(6.2) that we neglect any instrumental resolution uncertainties, thus ΔE depends on the width of the phonon mode (σ). We are then able to derive $\Delta\sigma \geq \frac{\hbar}{\Delta\tau} \rightarrow \tau \propto \sigma^{-1}$. We find $\Delta\sigma = 0.07$meV which corresponds to $\Delta\tau = 13.9$ns.
In Figure 7.5 we have fitted the intensity as

$$I \propto (n_B + 1) \ , \tag{7.1}$$

where n_B is the Bose-Einstein factor.
We see a deviation in the integrated intensities around T_N. Together with Figure 7.5, this shows

that the phonon mode is suppressed just around the magnetic phase transition. As we discussed earlier the shift can be understood as critical spin scattering of phonons [3]. And we have now seen that this critical spin scattering has a large effect on the phonon mode.

7.2 Magnetic Order

We scanned k around the $q(h\ k\ l) = (0\ -1\ 0)$ magnetic peak while slowly heating the crystal from 2K to 80K, to obtain the phase transition of our crystal. According to Le et all. [3], the magnetic phase transition is expected to be around $T_N = 75$K.

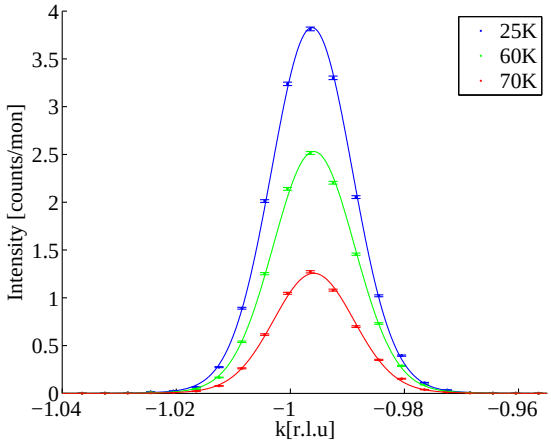

Figur 7.6: Rawdata of peaks ued to find T_N in Figure 7.7.

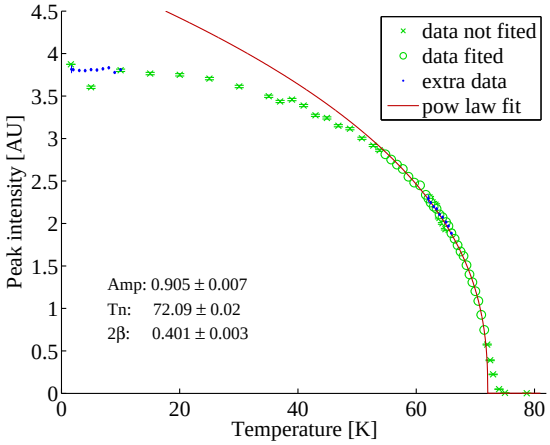

Figur 7.7: Magnetic Transition for $YMnO_3$. Raw data shown in Figure 7.6

A double gauss fit, with same center, was made for each scan. The amplitude from these fits have then been plotted as a function of temperature as seen in Figure 7.7. The selected data from 56K to 72K is fitted to the power law

$$I \propto \left(\frac{T_N - T}{T_N}\right)^{2\beta}$$

This yields $T_N = (72.09 \pm 0.02)$K, and $2\beta = (0.401 \pm 0.003)$[AU].
Our experimental T_N value lies differs with $\sim 3\%$ from Lee et al.'s value. This difference can be explained by Lee et al.'s losely determination of T_N. Looking at Roessli et al. [8], which have determined $T_N = 72.1 \pm 0.05$K, using the same experimental approach as we do. Roessle et al. [8] and our T_N are consistent but our critical exponent β is twice as big as Roessli et al.'s. This is due to different power law fits of the data.
We calculate the frustration index, eq(2.9), using the Curie-Weiss temperature $\theta_{CW} = -500$[3] of our crystal to be

$$f = \frac{|-500[\mathrm{K}]|}{72.09} = 6.93\ , \tag{7.2}$$

which is a rather large value of frustration. This large geometric frustration supports the previous discussion of critical spin fluctuations in our system.
We observe a deviation of our data relative to our powerlaw fit as we reach T_N. This can partly be explained as magnetic critical scattering, which is a broadening of the magnetic scattering cross-section as the magnetic phase transition temperature is reached from above[7]. From our study of the magnetic peaks in our crystal, Figure 6.7, we where able to see the magnetic broadening by doing a lorentz-gauss fit of the peaks.

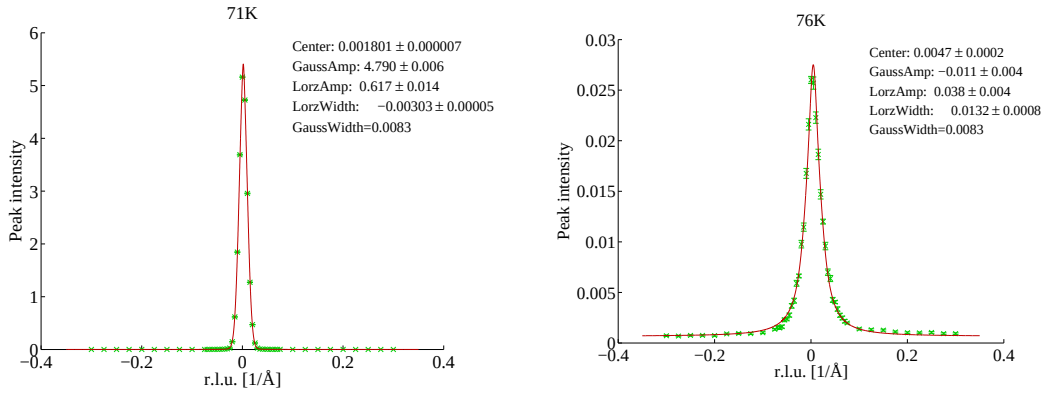

Figur 7.8: Widths of bragg peaks from Figure 6.7

Here we see a clear broadening of the fits as we are at a temperature around T_N hence we can determine that magnetic critical scattering effects will be observed in data around the magnetic phase transition temperature.

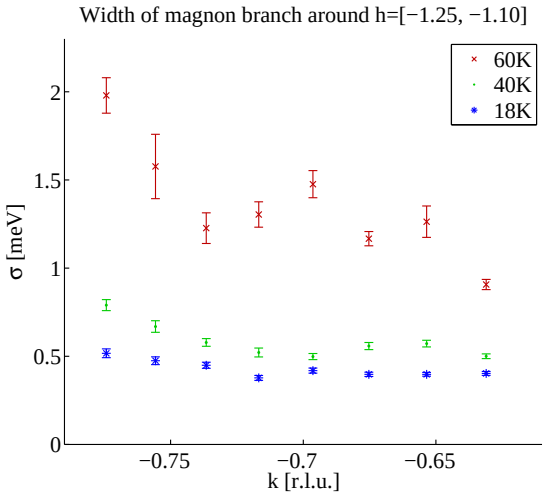

Figur 7.9: Width of magnon branch in Figure 6.8.

We evaluated the widths of the spinwave branch in the region $h[\text{r.l.u}] = [-1.25; -1.10]$ in Figure 6.8. The peaks have been projected on the k-axis using $q_k = (k + \frac{h}{2})\hat{k}$. We did this operation since the k-axis is approximately perpendicular to the observed branch. Comparing Figure 7.9 with Figure 7.3, the magnon width does not display any spontaneous shifts. This supports the assumption of phonon-magnon coupling since the magnon seems to behave differently whether there is a phonon present or not.

8 Conclusion

We see a clear interaction between the phonon and magnon branch, as they avoided crossing eachother on our colorplot, Figure 6.4, along with minor intensity signals between the branches. Additionally, we see a shift in both the magnon and phonon width around this avoid crossing point, Figure 7.1, Figure 7.3, which disappears when the phonons and magnons are alone, Figure 6.5 and Figure 7.9. This strongly motivates for a coupling between the phonon and magnon in our crystal, but I suggest further investigation of the area between the branches as well as for the avoided crossing point, before we have enough foundation to state that there exist phonon-magnon coupling. But we see strong evidence of phonon-magnon coupling.
We have measured a change in phonon width around the magnetic phase transition, up to $\Delta\sigma = 0.07$meV, see Figure 7.4, which could be documentation of phonon scattering due the critical spin fluctuations. This change lies just around T_N which supports the claim of phonon scattering due to magnetic excitations.

8.1 Outlook

Further investigation of the avoid crossing of the phonon and magnon branch would be very interesting, in order to understand what really happens at this point. This could be done using the instrument FLEXX, stationed at HZB, Berlin, since it is able to make scans over the avoid crossing point. Additionally, we can use polarized neutrons on FLEXX, which can distinguish between magnetic and nonmagnetic excitations. This would grant a better overview of what is happening at the avoid crossing point. Also, evaluation of the small intensity signals between the phonon-magnon branches could be fascinating, since this might be magnetoelectric coupling effects emerging from the two branches.

Litteratur

[1] Blundell, S., *Magnetism in Condensed Matter*, 1st edition, Oxford University Press, (2001).

[2] W. Eerenstein et al. *Nature 442, 759*, (2006).

[3] S. Lee et al *Nature 451, 805*, (2008).

[4] P. Sharma et al. *PRL 93, 177202*, (2004).

[5] C. Kittel, *Introduction to Solid State Physics*, 8th edition, John Wiley and Sona, Inc, (2005).

[6] D. J. Griffiths, *Introduction to Electrodynamics*, 3rd edition, Pearson Benjamin Cummings, (2008).

[7] M. Collins, *Magnetic Critical Scattering*, Oxford Express, (1989).

[8] B. Roessli et al. *JETP vol. 81 no. 6*, (2005).

[9] S. Petit, et al. *PRL 99, 266604*, (2007).

[10] T. J. Sato et al. *PRB 68, 014432*, (2003).

[11] K. Lefmann course notes: *Magnetic Neutron Scattering*, (2011).

[12] K. Lefmann et al. course notes: , itNeutron Scattering: Theory, Instrumentation, and Simulation., (2012).

[13] K. F. Wang et al. *Advances in physics - Multiferroicity*, Vol. 58, No. 4, Taylor and Francis, (2009).

[14] A. Muoz et al. *PRB 62, 9498*, (2000).

[15] M. Fiebig et al. *Letters to Nature 419, 01077*, (2002).

[16] X. Fabreges et al. *PRL 103, 067204*, (2009).

[17] H. M. Ronnow, ETH-Zurich & PSI, Switzerland.
http://lns00.psi.ch/mcworkshop/papers/Eiger_simulations_2006oct.pdf, visited (21/5-2013).

A EIGER - Energy scans of phonon-magnon branch

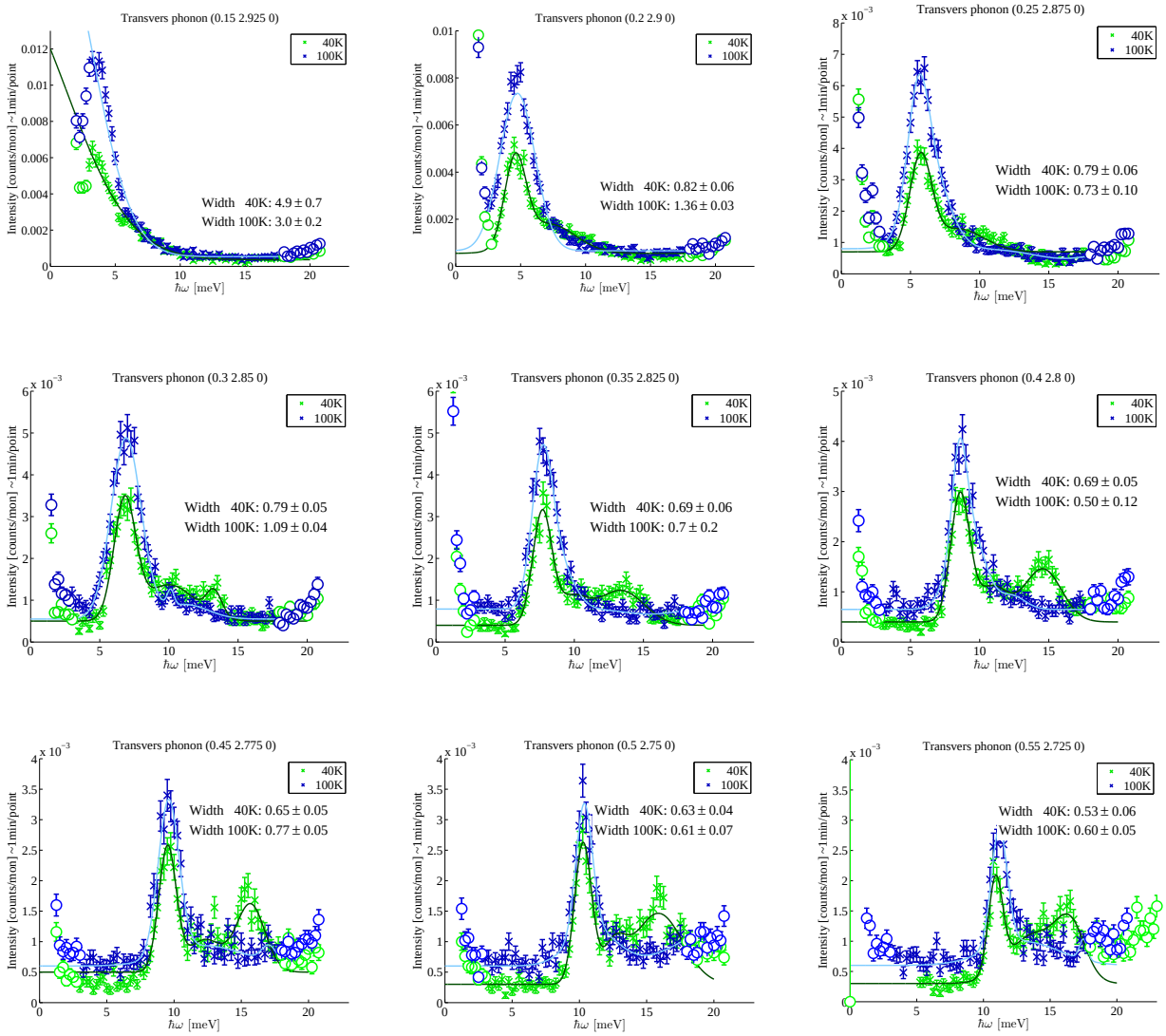

The black fit follows the green (40K) data, the lightblue fit follows the blue (100K) data.

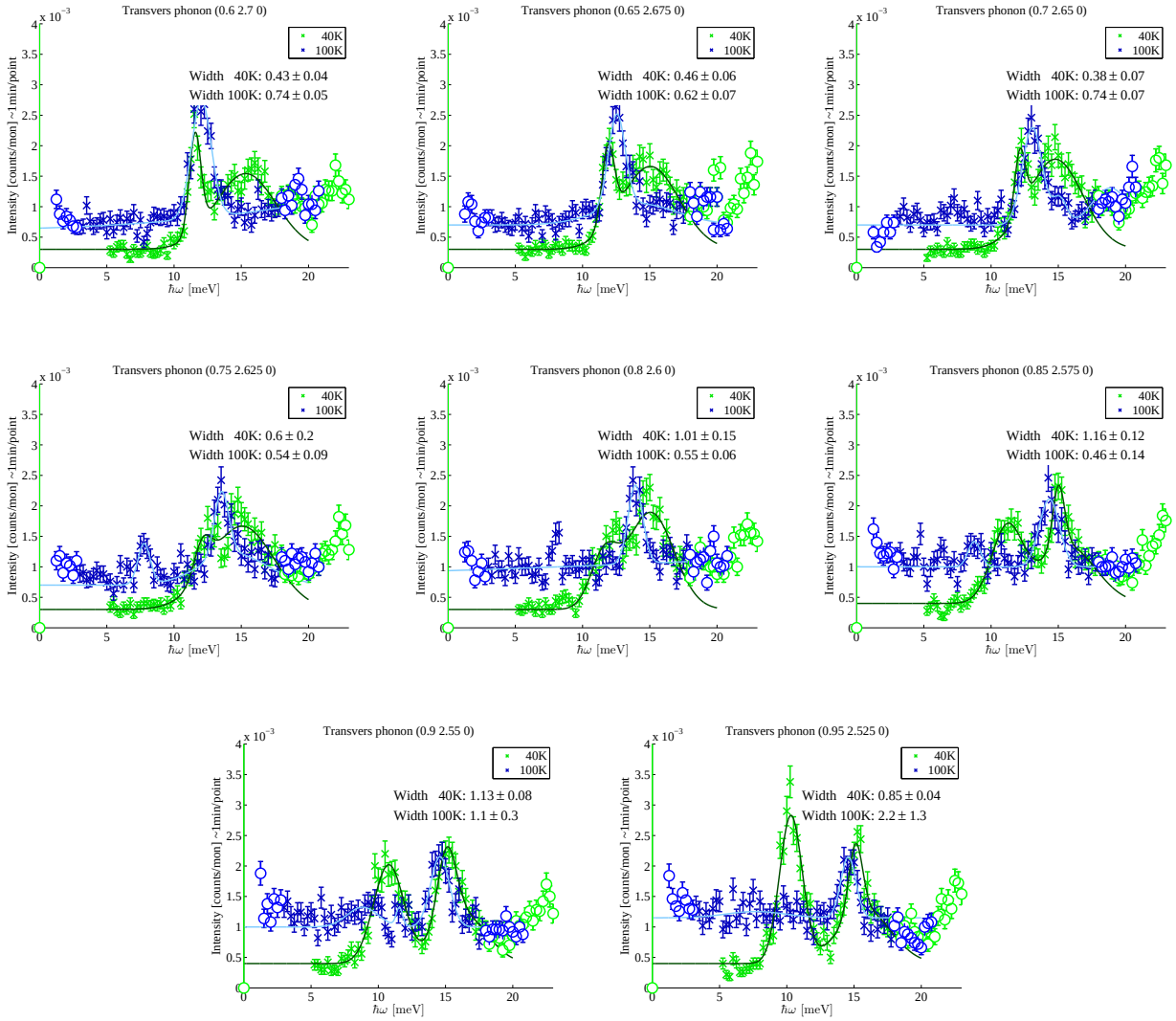

The black fit follows the green (40K) data, the lightblue fit follows the blue (100K) data.

B EIGER - Temperature scans at $q = (0.35\ 2.825\ 0)$

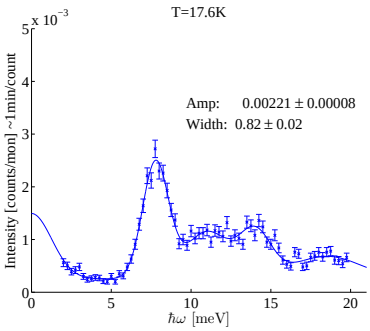

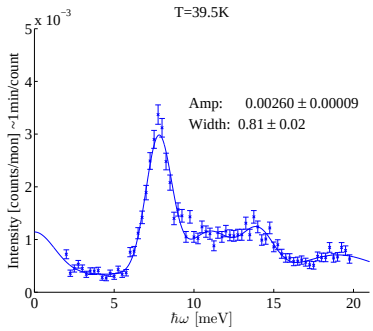

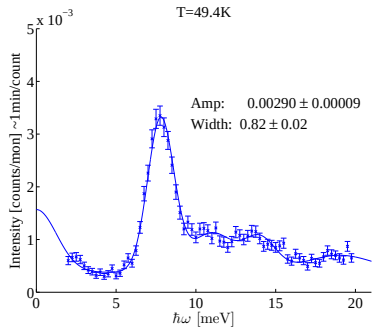

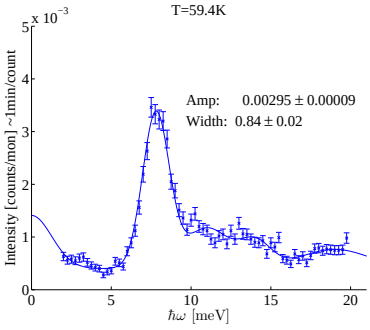

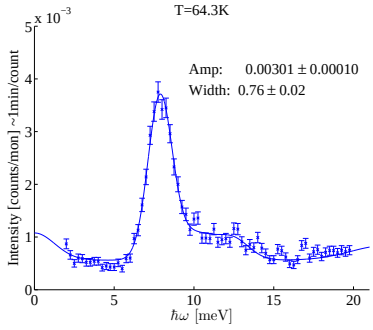

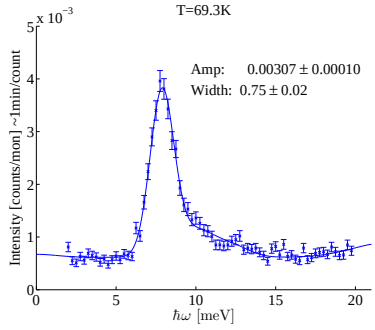

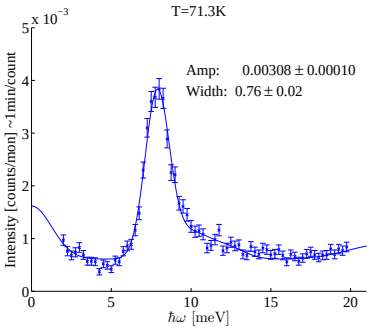

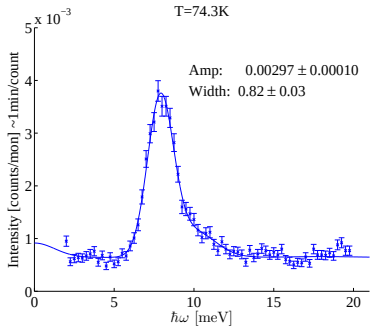

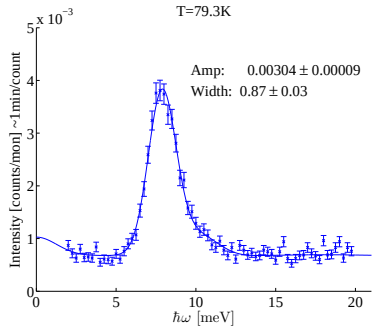

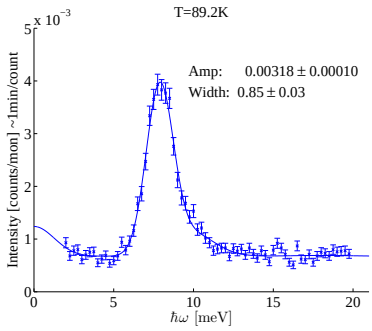

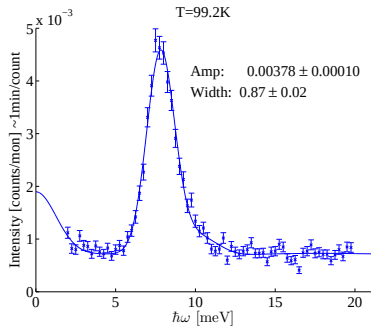

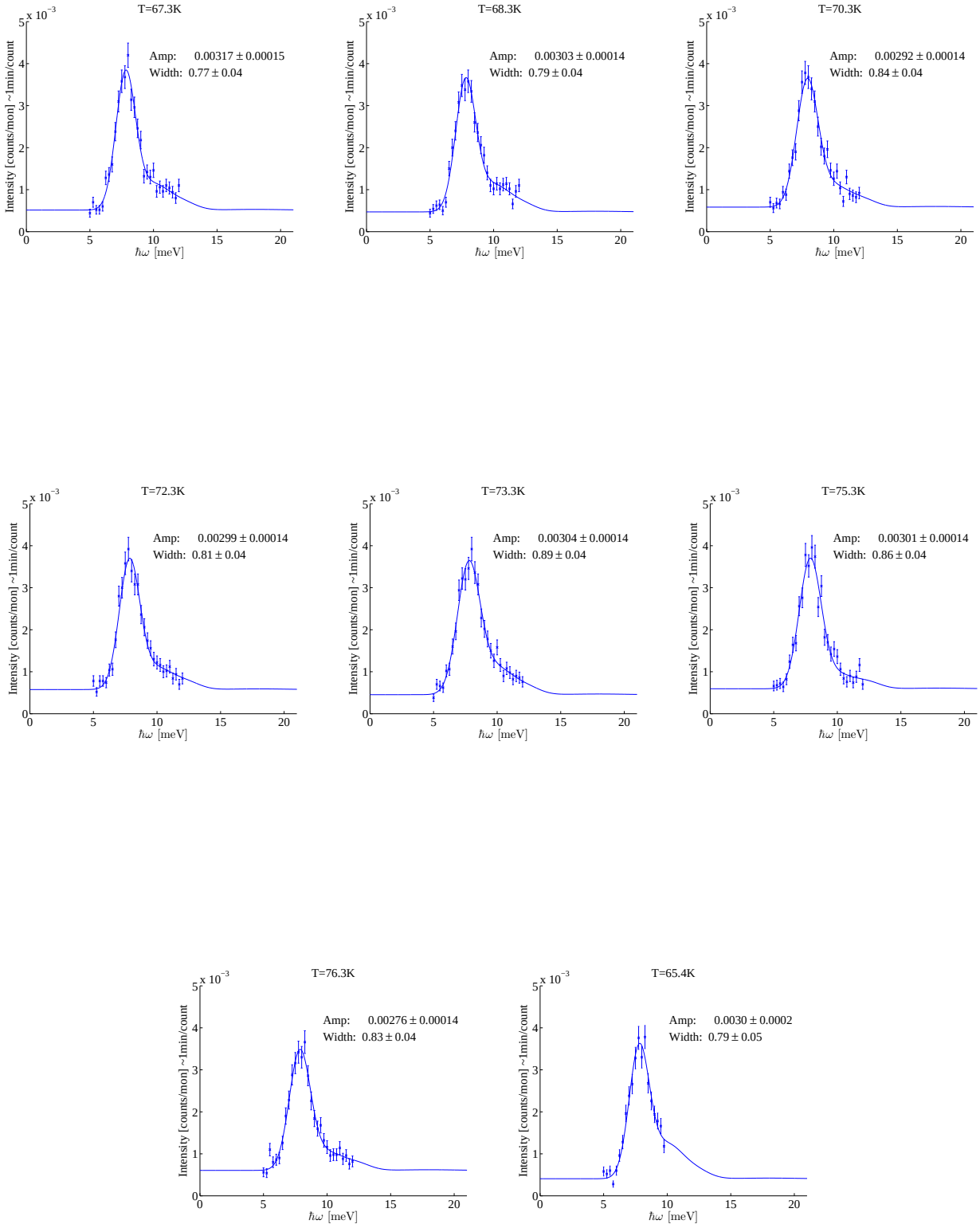

Figur B.1: Constant $q = (0.3\ 2.825\ 0)$, temperature variation, longitudinal phonon, transverse scans.

C RITA2 Bladenormalization

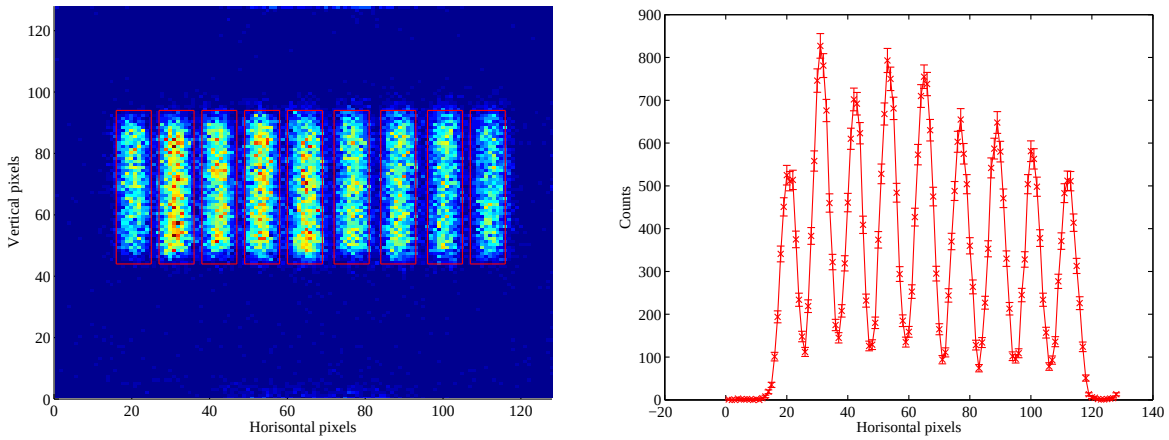

Figur C.1: Intensity plot showing RITA2's nine analyzer blades. (left) Intensity plot in 2D. (right) Intensity plot in 2D.

D RITA2 - Magnetic Peak at $q = (0\ -1\ 0)$

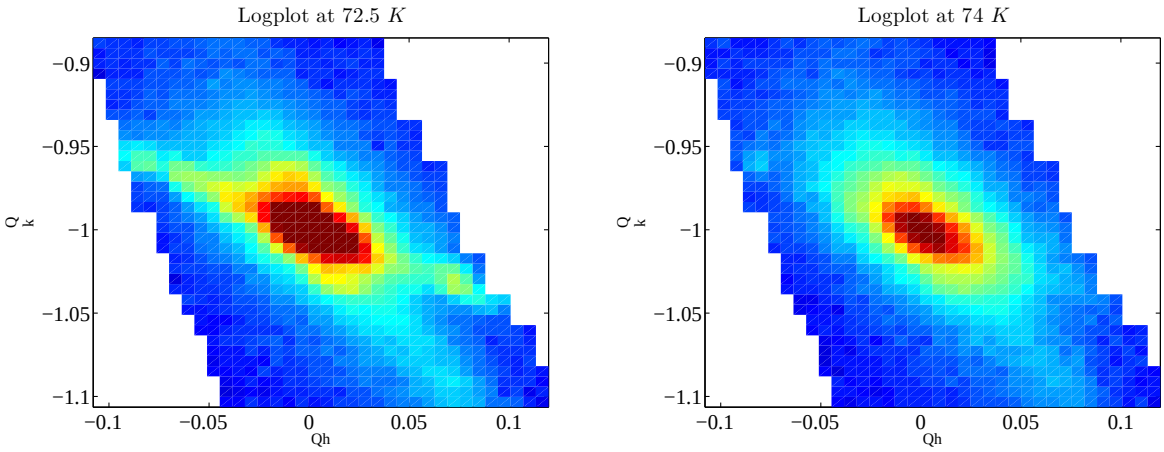

Figur D.1: Bragg peaks at $q = (0\ -1\ 0)$.

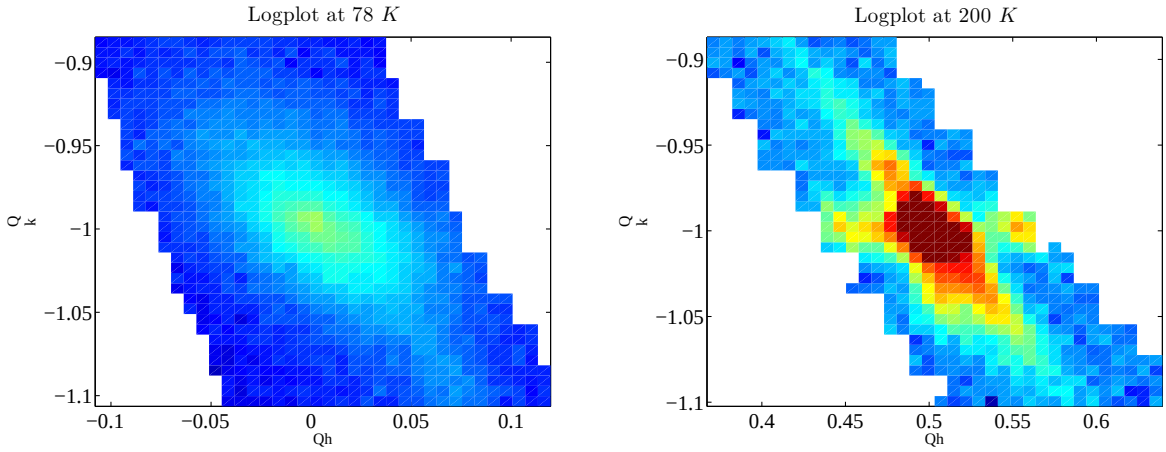

Figur D.2: Bragg peaks at $q = (0\ -1\ 0)$.

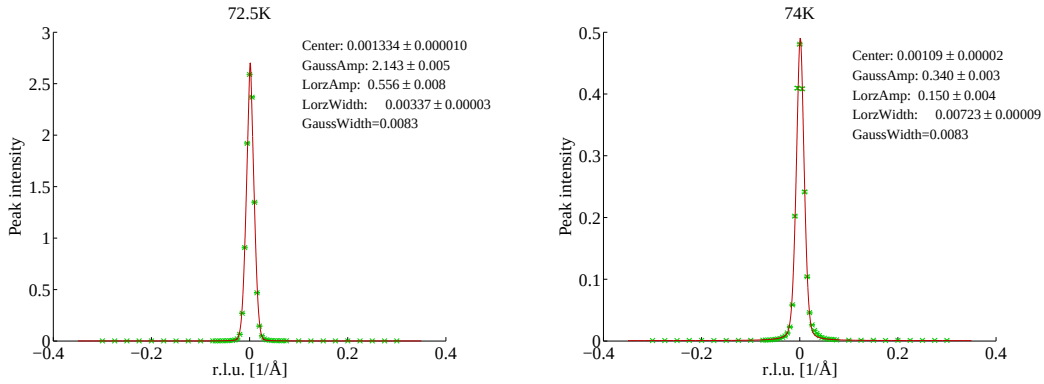

Figur D.3: Widths of bragg peaks from Figure D.1

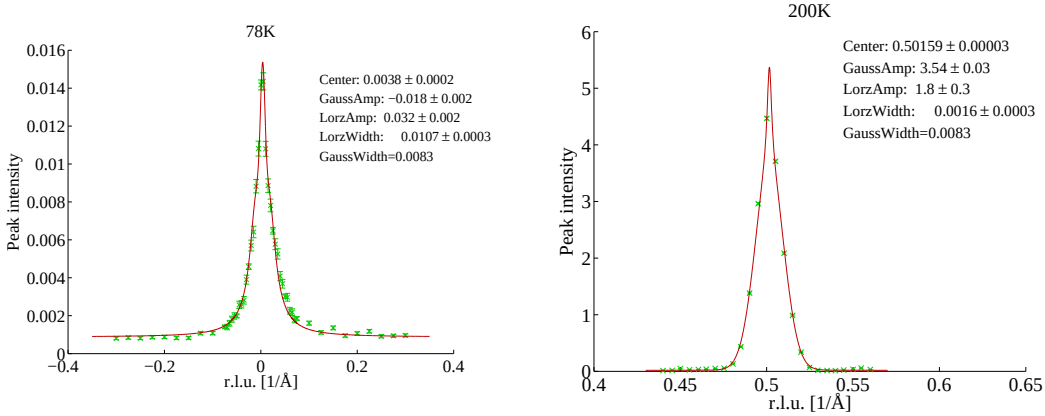

Figur D.4: Widths of bragg peaks from Figure D.2.